University of Reading

Improving climate change detection through optimal seasonal averaging: the case of the North Atlantic jet and European precipitation

Article

Published Version

Zappa, G., Hoskins, B. J. and Shepherd, T. G. ORCID: https://orcid.org/0000-0002-6631-9968 (2015) Improving climate change detection through optimal seasonal averaging: the case of the North Atlantic jet and European precipitation. Journal of Climate, 28 (16). pp. 6381-6397. ISSN 1520-0442 doi: 10.1175/JCLI-D-14-00823.1 Available at https://centaur.reading.ac.uk/40198/

It is advisable to refer to the publisher's version if you intend to cite from the work. See Guidance on citing.

To link to this article DOI: http://dx.doi.org/10.1175/JCLI-D-14-00823.1

Publisher: American Meteorological Society

All outputs in CentAUR are protected by Intellectual Property Rights law, including copyright law. Copyright and IPR is retained by the creators or other copyright holders. Terms and conditions for use of this material are defined in the End User Agreement.

University of Reading

www.reading.ac.uk/centaur

CentAUR

Central Archive at the University of Reading

Reading's research outputs online

Improving Climate Change Detection through Optimal Seasonal Averaging: The Case of the North Atlantic Jet and European Precipitation

GIUSEPPE ZAPPA, BRIAN J. HOSKINS, AND THEODORE G. SHEPHERD

Department of Meteorology, University of Reading, Reading, United Kingdom

(Manuscript received 4 December 2014, in final form 15 April 2015)

ABSTRACT

The detection of anthropogenic climate change can be improved by recognizing the seasonality in the climate change response. This is demonstrated for the North Atlantic jet [zonal wind at 850 hPa (U850)] and European precipitation responses projected by the climate models from phase 5 of CMIP (CMIP5). The U850 future response is characterized by a marked seasonality: an eastward extension of the North Atlantic jet into Europe in November–April and a poleward shift in May–October. Under the RCP8.5 scenario, the multimodel mean response in U850 in these two extended seasonal means emerges by 2035–40 for the lower-latitude features and by 2050–70 for the higher-latitude features, relative to the 1960–90 climate. This is 5–15 years earlier than when evaluated in the traditional meteorological seasons (December–February and June–August), and it results from an increase in the signal-to-noise ratio associated with the spatial coherence of the response within the extended seasons. The annual mean response lacks important information on the seasonality of the response without improving the signal-to-noise ratio. The same two extended seasons are demonstrated to capture the seasonality of the European precipitation response to climate change and to anticipate its emergence by 10–20 years. Furthermore, some of the regional responses (such as the Mediterranean precipitation decline and the U850 response in North Africa in the extended winter) are projected to emerge by 2020–25, according to the models with a strong response. Therefore, observations might soon be useful to test aspects of the atmospheric circulation response predicted by some of the CMIP5 models.

1. Introduction

The evidence that climate is changing as a result of anthropogenic greenhouse gas emissions continues to strengthen (Bindoff et al. 2013). For thermodynamic aspects of climate, such as surface temperature and Arctic sea ice extent, significant observed trends have already been detected and attributed to increasing levels of greenhouse gases and changing aerosol concentrations (Hegerl et al. 1997; Stott 2003; Barnett et al. 2005). On the other hand, projected changes in atmospheric circulation have not yet been detected in the observations, thus limiting the confidence in the future projections. This constitutes a key challenge for climate science (Shepherd 2014) as future changes in atmospheric circulation, midlatitude jets, and storm tracks (Chang et al. 2012; Barnes and Polvani 2013; Zappa et al. 2013) may lead to large socioeconomic impacts by modulating regional storminess and precipitation (Pinto et al. 2012). It is therefore of great interest to find any approach that might allow an earlier detection of the atmospheric circulation response to climate change in observations.

The main limitation to the detection of the atmospheric circulation response to climate change is the large natural variability that characterizes the climate system (Hawkins and Sutton 2009; Deser et al. 2012). Natural variability is internal to the atmosphere–ocean–sea ice coupled system and it occurs independently of changes in external forcing. Deser et al. (2012) suggest that future trends in precipitation and sea level pressure at single locations will be dominated by natural climate variability for at least 50 years. Local trends in temperature can also be modulated by natural variability (Deser et al. 2014), although the trends are more robust than for precipitation or sea level pressure. Furthermore, the climate change response can project onto modes of atmospheric natural variability, making it more difficult to distinguish between the forced and internal components (Palmer 1999). For example, it is still unclear whether the observed trend in North Atlantic

Corresponding author address: Giuseppe Zappa, Department of Meteorology, University of Reading, Earley Gate, P.O. Box 243, Reading RG6 6BB, United Kingdom.
E-mail: g.zappa@reading.ac.uk

DOI: 10.1175/JCLI-D-14-00823.1

© 2015 American Meteorological Society

sea level pressure between 1960 and 2000 was externally forced (Shindell et al. 1999; Gillett et al. 2003) or was primarily generated by internal climate variability (Osborn 2004; Semenov et al. 2008; Wallace et al. 2012).

A standard approach to increase the ratio between the amplitude of the expected climate change response (the signal) compared to the amplitude of the fluctuations due to natural variability (the noise) is to take spatial averages over global, hemispheric, or continental scales (e.g., Stott 2003; Gillett and Stott 2009; Balan Sarojini et al. 2012). In this approach, an average is taken over grid points where fluctuations due to natural variability are only weakly correlated with each other, so that the noise is reduced. For example, Gillett and Stott (2009) detected an externally forced increase in the zonal-mean mean sea level pressure in the tropics, and Zhang et al. (2007) detected externally forced changes in the precipitation over land when spatially averaged over four different zonal bands. However, spatial averaging has less value for regional analysis, given the constraints on the extent of the averaging area.

In a similar way, signal-to-noise ratio can be increased by temporal averaging through the year. For example, it is standard practice in detection and attribution studies to consider meteorological-season means rather than monthly means (e.g., Gillett et al. 2005; Gillett and Stott 2009; Noake et al. 2012; Barkhordarian et al. 2013; Marvel and Bonfils 2013), which reduces the noise from intraseasonal variability while still representing the seasonal cycle. Taking annual means (Bindoff et al. 2013) can reduce the noise even more but loses any seasonal information. Since there is no a priori reason to expect the meteorological seasons to best characterize the climate change response, other choices may be more informative. Indeed, several authors (e.g., Wallace et al. 2012; Iles et al. 2013; Seager et al. 2014) have considered extended cold and warm seasons (6-month averages) in their characterization of the climate change response, but to our knowledge there has not been a systematic exploration of the optimal choice of temporal averaging from the perspective of climate change detection. The basic trade-off is between how much signal is lost as the noise is reduced through temporal averaging, and this depends on the seasonality of the climate change response.

Thus, the aim of this paper is to examine the potential of using information on the seasonality of the climate change response to identify optimal temporal averages that increase the signal-to-noise ratio and may thereby facilitate climate change detection in the observations and help constrain model projections. This will be explored first for the future response of the zonal wind at 850 hPa (U850) in the North Atlantic and European region as projected by the climate models participating in phase 5 of the Coupled Model Intercomparison Project (CMIP5). U850 is related to the behavior of the North Atlantic eddy-driven jet, which is an important driver of the weather in the European region (Woollings et al. 2010). No anthropogenic climate change signal has yet been clearly detected for this field in the observations, although model projections suggest that substantial changes may occur in the future (Barnes and Polvani 2013; Simpson et al. 2014). The analysis will then be extended to examine the seasonality of projected changes in mean precipitation, with a particular focus on Europe. The impact of optimal temporal averages on climate change detection will be quantified in terms of the time of emergence of climate change. The time of emergence is generally defined as the time interval needed before the climate change response becomes larger than the random fluctuations induced by internal climate variability, and different approaches have been proposed to quantify it (Christensen et al. 2007; Giorgi and Bi 2009; Mahlstein et al. 2011; Hawkins and Sutton 2012). The uncertainty on the time of emergence due to differences in the model responses will also be estimated (Hawkins and Sutton 2012).

The structure of the paper is as follows. Section 2 introduces the data and methods, including a discussion of how we define time of emergence. In section 3 the seasonality of the CMIP5 multimodel mean response in U850 is analyzed and two extended seasons that best capture the climate change response are identified. In section 4, the time of emergence of the U850 climate response in the meteorological and extended seasonal averages are quantified and compared. In section 5, the results are interpreted in relation to the signal-to-noise ratio of the climate response. Section 6 extends the analysis introduced for U850 to the precipitation response. The conclusions are given in section 7.

2. Data and methods

a. *CMIP5 models*

The 35 CMIP5 coupled climate models listed in Table 1 are considered in this study. The climate change response is evaluated for the representative concentration pathway 8.5 (RCP8.5) emission scenario (Taylor et al. 2012). This corresponds to a future scenario with little climate change mitigation in the twenty-first century. If available, multiple ensemble members from each model are averaged before computing the individual models' climate change response. The multimodel mean is computed as an unweighted mean of the individual CMIP5 model responses interpolated to a common T42 Gaussian grid using bilinear interpolation for U850 and conservative

TABLE 1. List of CMIP5 models considered in the study. For each model the number of analyzed runs in the historical (HIST) and RCP8.5 simulations are indicated. (Expansions of acronyms are available online at http://www.ametsoc.org/PubsAcronymList.)

	Basic information		No. of runs	
	Model name	Institution	HIST	RCP8.5
1	ACCESS1.0	CSIRO and BOM, Australia	1	1
2	ACCESS1.3		3	1
3	BCC_CSM-1.1	BCC, China	3	1
4	BCC_CSM-1.1(m)		3	1
5	BNU-ESM	Beijing Normal University, China	1	1
6	CCSM4	NCAR, United States	6	6
7	CESM1(CAM5)	National Science Foundation, DOE, and NCAR, United States	3	3
8	CESM1(WACCM)		4	3
9	CMCC-CESM	CMCC, Italy	1	1
10	CMCC-CM		1	1
11	CMCC-CMS		1	1
12	CNRM-CM5	Centre National de Recherches Météorologiques, France	5	3
13	CSIRO Mk.3.6.0	CSIRO, Australia	10	10
14	CanESM2	CCCma, Canada	5	5
15	EC-EARTH	EC-Earth Consortium, Europe	5	5
16	FGOALS-g2	LASG, China	4	1
17	FIO-ESM	First Institute of Oceanography, China	3	3
18	GFDL CM3	GFDL, United States	5	1
19	GFDL-ESM2G		1	1
20	GFDL-ESM2M		1	1
21	GISS-E2-H	NASA GISS, United States	5	1
22	GISS-E2-R		5	1
23	HadGEM2-ES	Met Office Hadley Centre, United Kingdom	4	4
24	HadGEM2-CC		3	3
25	INM-CM4	Institute of Numerical Mathematics, Russia	1	1
26	IPSL-CM5A-LR	IPSL, France	5	4
27	IPSL-CM5A-MR		3	1
28	IPSL-CM5B-LR		1	1
29	MIROC-ESM	JAMSTEC, Atmosphere and Ocean Research Institute (AORI) at the University of Tokyo, and National Institute for Environmental Studies, Japan	3	1
30	MIROC-ESM-CHEM		1	1
31	MIROC5		5	3
32	MPI-ESM-LR	Max Planck Institute for Meteorology, Germany	3	3
33	MPI-ESM-MR		3	1
34	MRI-CGCM3	Meteorological Research Institute, Japan	3	1
35	NorESM1-m	Norwegian Climate Centre, Norway	3	1

remapping for precipitation (Jones 1999). To explore the evolution of the climate change response through the twenty-first century the historical simulations (from 1960 to 2005) and the RCP8.5 simulations (from 2006 to 2100) of each model have been merged together by concatenating the time series.

The magnitude of the internal climate variability simulated by the CMIP5 models has been tested against the variability found in observational datasets. In particular, the variability in U850 has been tested against the variability found in the recently released Japanese 55-year Reanalysis (JRA-55) for the period 1958–2013 (Kobayashi et al. 2015) and that found in the ECMWF interim reanalysis (ERA-Interim, hereafter ERAI) for the period 1979–2013 (Dee et al. 2011). Furthermore, internal climate variability in the precipitation has been evaluated using the CPC Merged Analysis of Precipitation (CMAP) dataset (Xie and Arkin 1997) and the Global Precipitation Climatology Project (GPCP) precipitation dataset (Adler et al. 2003), both for 1979–2013. The GPCP and CMAP datasets combine satellite-derived information with surface gauge data to generate a climatology of observed precipitation over both land and oceanic regions.

b. *Signal-to-noise ratio and time of emergence*

The definitions of signal-to-noise ratio and time of emergence of climate change used in this study are similar to those described in Christensen et al. (2007). At a given lead time, the signal $\beta(t)$ is evaluated as the CMIP5 multimodel mean difference between a 30-yr mean in the RCP8.5 scenario and a reference 30-yr mean in the historical simulations (1960–90). A range of lead times

are considered by shifting the future time window in the RCP8.5 scenario from 1980–2010 to 2070–2100 in 5-yr steps. By considering a multimodel mean, the signal is well sampled and only weakly affected by internal climate variability. The years 1960–90 are chosen as the reference period as regular radiosonde observations are available on a global scale from this period onward (Kobayashi et al. 2015). The sensitivity to using a later reference period (1979–2009), when satellite information becomes available, will be discussed for the precipitation projections.

The internal variability, here seen as noise, is estimated from the CMIP5 data according to the framework introduced by Sansom et al. (2013). In this framework, internal variability is quantified as the standard deviation σ of the fluctuations of the 30-yr mean climate due to different initial conditions of the model simulations. The fluctuations are evaluated by pooling together the anomalies in the mean climate in the historical simulations of each ensemble member relative to the respective model ensemble mean [see Eq. (A1) in the appendix]. Using this approach, a single estimate of internal variability is generated for the whole multimodel ensemble. This is appropriate because the time of emergence depends on the variability of the real climate system, not of particular models. Observations cannot be reliably used to estimate variability of 30-yr means without strong assumptions on autocorrelations, so our approach is to use the pooled model variability as the primary estimate and to check that it is consistent with that inferred from observations. More details on this methodology and a discussion of the assumptions made are presented in the appendix.

Following Christensen et al. (2007), the time of emergence is here defined as the time interval needed before the multimodel mean climate change signal is significant at the 5% level relative to the noise of a single realization (σ). This is estimated as the first lead time τ when the signal-to-noise ratio condition

$$\left|\frac{\beta(\tau)}{\sigma\sqrt{2}}\right| \geq 1.96 \Rightarrow |\beta(\tau)| \geq 2.77\sigma \qquad (1)$$

is satisfied. In Eq. (1), thanks to the large number of ensemble members contributing to estimate σ, we have considered the test statistic β/σ to be normally distributed.

This definition of time of emergence has two properties that ease its interpretation:

- By the time of emergence, the response of a single realization is likely (>95%) to have the same sign of the climate change response, regardless of internal variability.
- By the time of emergence, there is a 50% chance that a single realization shows a statistically significant response at the 5% level. Note that a statistically significant response might be detected earlier if the random internal variability combines to amplify the forced climate change response, or later if it opposes the forced climate change response.

The first property is particularly useful in the context of testing climate model projections. If, by the time of emergence, observations show a response of opposite sign to that projected by the models, we can conclude that the model projections are likely (>95%) to be unrealistic and either miss or exaggerate the climate response. As illustrated in section 4c, this property might soon be applied to use observations to provide an upper bound on the most extreme model projections in some regions.

A different approach was proposed in Hawkins and Sutton (2012), who defined the time of emergence as the first lead time when the climate response becomes "large," by a factor of 1 or 2, compared to the standard deviation of the year-to-year variability. While the Hawkins and Sutton (2012) definition of time of emergence is useful to interpret the emergence of climate impacts, it lacks the two useful properties given above. Therefore, we find the Christensen et al. (2007) approach more appropriate for this study as it allows a statistical interpretation of when climate change might be detected and model projections tested using observations.

3. The seasonality of the North Atlantic 850-hPa zonal wind response

Figure 1 shows the CMIP5 multimodel mean end-of-century U850 response (2070–99 minus 1960–90) separately computed for each calendar month. Thanks to the large number of models and ensemble members averaged in the multimodel mean, the monthly climate change response is well sampled and only weakly affected by internal climate variability. This has been verified by examining the sensitivity of Fig. 1 to using only one ensemble member per model, which proved to be small (not shown).

Figure 1 reveals that the multimodel mean response in U850 smoothly evolves through the annual cycle but it also shows that some spatial patterns tend to persist for a number of consecutive months. From December to April, the mean response features an eastward wind change over central Europe and a westward wind change over North Africa. This dipole between Europe and North Africa is largest in January and smallest in April, and it persists for the whole period at nearly unchanged locations. With the exception of April, the U850 response in the North Atlantic region is weaker than in Europe and it shows little spatial coherence between the different months. A slight westward wind response is also found in

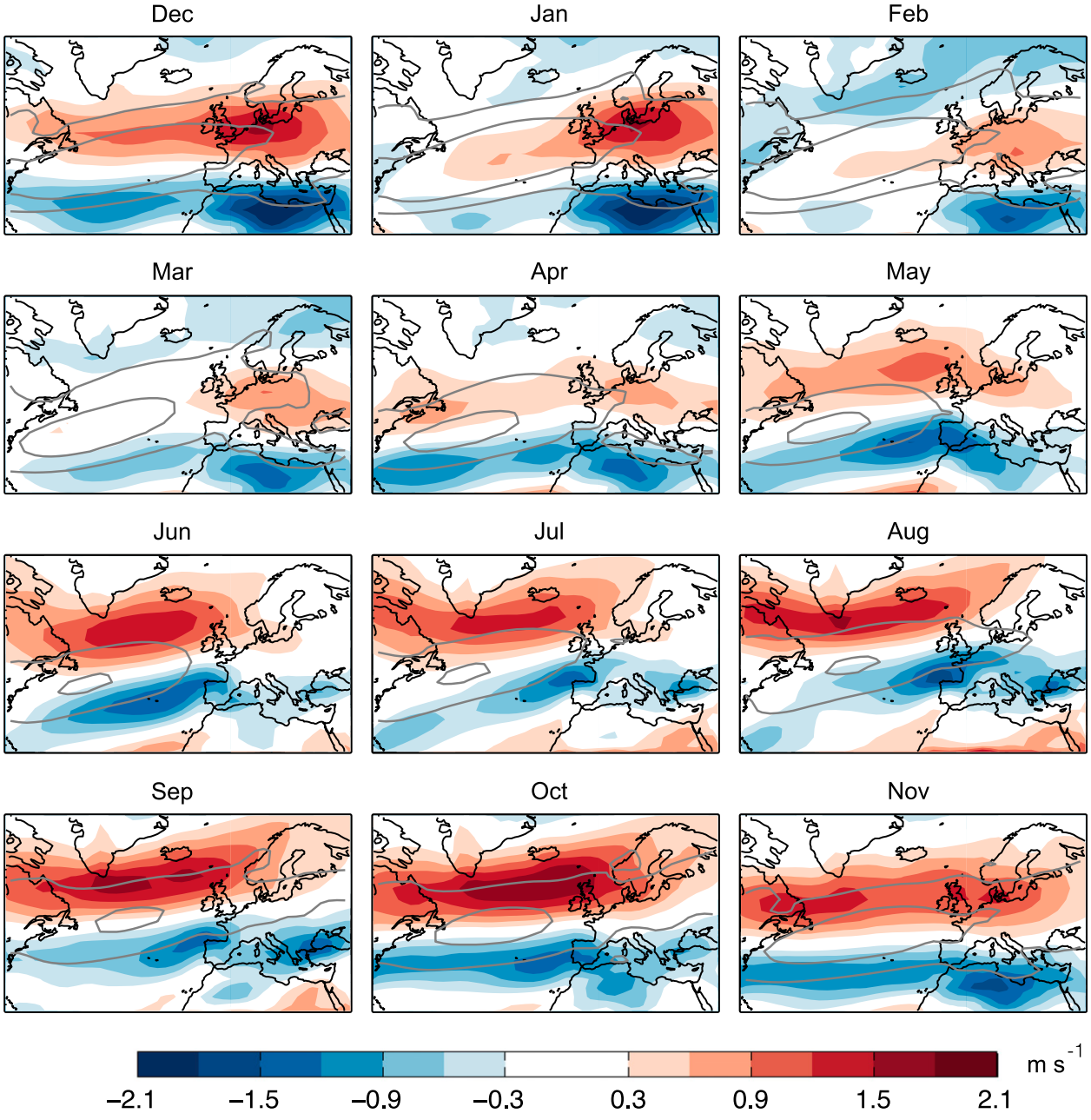

FIG. 1. CMIP5 multimodel mean climate response (shading) in the zonal wind at 850 hPa by the end of the twenty-first century under the RCP8.5 scenario. The climate response is separately presented for each individual calendar month. Gray contours correspond to the 4 (outer) and 8 (inner) m s^{-1} isotachs of the zonal wind at 850 hPa in the historical period (1960–90) in the multimodel mean.

the North Atlantic section of the Arctic Ocean. Overall, the U850 response is primarily suggestive of an eastward extension of the North Atlantic jet into Europe, which has also been previously identified in winter [December–February (DJF)] in other studies (Pinto et al. 2007; Zappa et al. 2013; Simpson et al. 2014).

A qualitatively different response in U850 is found from May to October. In this period, the multimodel mean response primarily consists of an intensification of the westerlies north of the climatological North Atlantic jet latitude (gray contours) and of a weakening to the south of it. The pattern of the response is suggestive of a poleward shift of the jet, and the response is found to be strongest in September and October. This is consistent with the results from Simpson et al. (2014), who identified a very robust poleward shift of the North

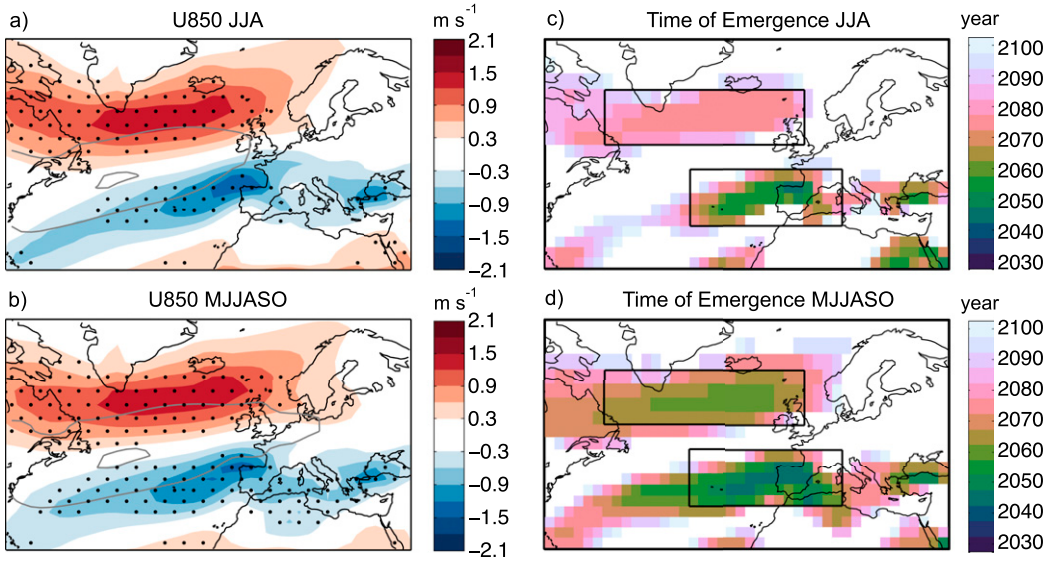

FIG. 2. Multimodel mean end-of-century U850 response separately computed for the (a) meteorological summer (JJA) and (b) extended summer (MJJASO) time averages. (c),(d) The time of emergence of the U850 response evaluated for the time periods in (a) and (b), respectively. In (a) and (b), stippling is applied where at least 90% of the models show a response of the same sign for the end-of-century climate change response, and the gray contours correspond to the 4 (outer) and 8 (inner) m s^{-1} isotachs of U850 in the historical period in the multimodel mean.

Atlantic jet, as measured by the latitude of strongest westerlies, in autumn [September–November (SON)] in the CMIP5 models.

The November response is intermediate between that of December–April and that of May–October. In particular, the November response features both a poleward shift of the jet in the North Atlantic and a dipole response between central Europe and North Africa, which are the main characteristics of the summer and winter responses, respectively.

Overall, these results suggest that the future response of the North Atlantic eddy-driven jet to climate change involves two different dynamical responses: a poleward shift from May to November and an eastward extension into Europe from November to April. This suggests that splitting the year into an extended winter and an extended summer season is dynamically sound for detecting zonal wind changes in the North Atlantic and Europe. November could be included in either of the two extended seasons; for simplicity, it will be included in the extended winter period so as to split the year into two 6-month periods [May–October (MJJASO) and November–April (NDJFMA)]. These will be referred to as extended summer and winter, respectively. This partitioning of the year into extended seasons has been used in some previous studies (e.g., Wallace et al. 2012; Seager et al. 2014), although motivated by different arguments (see discussion in the conclusions).

4. The time of emergence of the U850 response

The previous section showed that the U850 response in the CMIP5 climate models can be well described by two 6-month extended seasonal averages. In this section, we explore the potential to detect the climate change response in these extended seasonal averages compared with the meteorological seasons. The results will be separately presented for summer and winter. The uncertainty due to differences in the model responses will then be discussed.

a. Summer

Figures 2a and 2b show the multimodel mean end-of-century U850 response for the meteorological [June–August (JJA)] and extended (MJJASO) summertime averages. The U850 response in MJJASO strongly resembles that found in JJA, and they both show the dipolar response associated with the poleward shift of the North Atlantic jet. This suggests that little information is lost by extending the season length. Furthermore, stippling is added to Figs. 2a and 2b where at least 90% of the models agree on the sign of the projected change. This shows that there is high consensus on the projected poleward shift of the jet in both JJA and MJJASO across the CMIP5 models, but the region over which there is consensus is extended in MJJASO.

The time of emergence of the CMIP5 multimodel mean U850 response is presented in Figs. 2c and 2d for JJA and MJJASO, respectively. The interpretation of

TABLE 2. Time of emergence (year) of the climate change response in U850, area averaged in the four regions delimited by boxes in Figs. 2c,d and 3c,d, relative to the 1960–90 climatology. The columns give the time of emergence evaluated for the extended season, the standard meteorological season, and the difference between the two. The mean response row reports the time of emergence evaluated for the multimodel mean response, while the uncertainty ranges due to differences in the model responses are reported in the weak response and strong response rows.

Response	MJJASO	JJA	Diff	NDJFMA	DJF	Diff
	Northern North Atlantic			Central Europe		
Weak	2080	>2100	<−25	>2100	>2100	—
Mean	2055	2070	−15	2070	2085	−15
Strong	2030	2045	−15	2030	2030	0
	Southeastern North Atlantic			North Africa		
Weak	2080	2100	−20	2080	2095	−15
Mean	2040	2045	−5	2035	2045	−10
Strong	2020	2025	−5	2025	2035	−10

the time of emergence is only meaningful where the different CMIP5 models show consistent projections. Therefore, the discussion of the results will be limited to the areas where at least 90% of the models agree on the direction of change by the end of the twenty-first century (2070–2100 minus 1960–90). The signals associated with the poleward shift of the jet are both projected to emerge within the twenty-first century in JJA (Fig. 2c). In particular, at the individual grid points the weakening of the westerlies south of the jet in the southeastern North Atlantic (including Iberia) emerges by about 2055, and the strengthening of the westerlies to the north of the jet in the northern North Atlantic emerges by about 2075.

Despite the similar signals, the time of emergence of the MJJASO mean response is nearly everywhere advanced relative to that found for JJA (cf. Figs. 2c and 2d). This is due to an increase in the signal-to-noise ratio of the climate response, which will be discussed in detail in section 5. To better quantity the benefit from extending the seasonal average, we have computed the time of emergence of the U850 response area averaged in the two regions where the climate change signal is largest: the northern North Atlantic and the southeastern North Atlantic (see boxes in Figs. 2c,d). The estimated time of emergence of the area-averaged response in the two regions is reported in Table 2 in the rows labeled "mean response." Table 2 shows that the time of emergence decreases from 2070 (JJA) to 2055 (MJJASO) in the northern North Atlantic and from 2045 (JJA) to 2040 (MJJASO) in the southeastern North Atlantic. These values are about five years lower than the earliest time of emergence found at the individual grid points, as the area averaging allows a further increase in the signal-to-noise ratio of the climate response. Overall, these results are indicative of a benefit of about 5–15 years for the detection of the climate change response in the zonal wind by considering MJJASO compared with JJA.

b. Winter

Figures 3a and 3b show the multimodel mean end-of-century U850 response for the meteorological (DJF) and extended (NDJFMA) wintertime averages. Similar to what is found for summer, the extended winter response in U850 strongly resembles that found for DJF, although the amplitude is slightly reduced. The response is dominated by the strengthening of the westerlies over central Europe and by an opposite change over North Africa. High consensus across the CMIP5 models (stippling) is found with regard to the weakened zonal wind response in North Africa (Figs. 3a,b) and, although to a more limited extent, with regard to the strengthened westerlies in central Europe. In contrast, high consensus is generally not found in the North Atlantic except in the southwest, near Florida, in NDJFMA.

Figures 3c and 3d show the time of emergence of the climate change response for DJF and NDJFMA, respectively. The winter dipole in the U850 response between central Europe and North Africa is projected to emerge within the twenty-first century for both the DJF and NDJFMA time means. However, as found for summer, the time of emergence of climate change is advanced by extending the seasonal average to NDJFMA in both these two regions. This is quantified in Table 2, which presents the time of emergence of the area-averaged U850 response in central Europe and North Africa (see boxes in Figs. 3c,d). The results show that the time of emergence decreases from 2085 (DJF) to 2070 (NDJFMA) in central Europe and from 2045 (DJF) to 2035 (NDJFMA) in North Africa.

c. Model uncertainty

For a given emission scenario, a main source of uncertainty on the time of emergence of climate change is due to differences in the responses of the models. This contribution is termed model uncertainty in Hawkins and Sutton (2009). In particular, even where models are consistent on the direction of change, substantial intermodel differences can exist in the amplitude of the response. A stronger or weaker response implies that the signal might be detected earlier or later, respectively, compared to the multimodel mean response. This is analyzed in detail for the four regions identified in the previous sections.

Figures 4a–d show the temporal evolution of the extended seasonal mean U850 multimodel mean response (black dashed lines) area averaged in the four regions identified in Figs. 2d and 3d. For each region, the horizontal red line marks the 2.77σ noise level [see Eq. (1)],

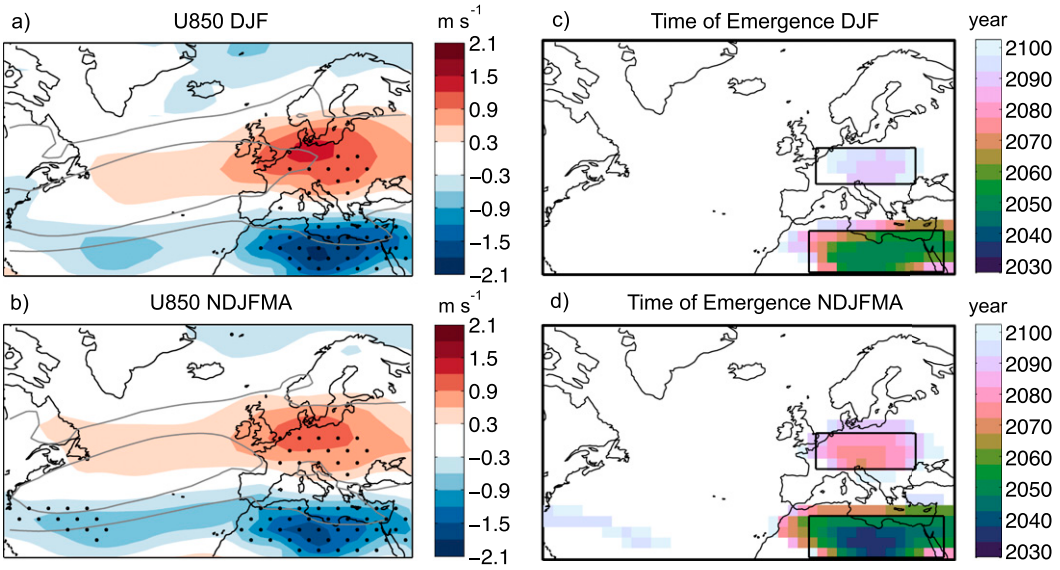

FIG. 3. As in Fig. 2, but for the meteorological winter (DJF) and the extended winter (NDJFMA) time averages.

which gives the magnitude of the internal climate variability on the 30-yr mean response in a single realization. In other words, in the absence of climate change, the response of any realization would be unlikely (<5%) to exceed the level delimited by the red line. The intersection between the red line and the black dashed line gives the time of emergence of the multimodel mean response [Eq. (1)].

To quantify the model uncertainty on the amplitude of the response, the gray dashed lines show the multimodel mean of the 20% of models with the strongest and weakest end-of-century[1] climate change response. Because of the small number of averaged models (seven per group) there is some residual internal variability, which shows as wiggles in the gray lines. To filter this residual variability, a third-order polynomial (Fig. 4; black line) is fit to the weak and strong model responses for the period 2010–2100 in a least squares sense. Therefore, the intersections between the red line and the black lines delimit the uncertainty range on the time of emergence due to differences in the model responses (Fig. 4; pink shading).

It is found that the uncertainty in the time of emergence of climate change due to differences in the model responses is substantial and that it differs between the different regions and seasons. The smallest uncertainty (about [−25, +25] yr) is found for the increase of U850 in the northern North Atlantic in the extended summer (Fig. 4a), which emerges by 2030 in the models with a stronger response and by 2080 in those with a weaker response. Models are therefore consistent in indicating that the strengthening of the zonal wind to the north of the jet will emerge in the twenty-first century, although the timing is uncertain. In contrast, Fig. 4c shows that while the increase of U850 in central Europe in the extended winter also emerges by 2030 in the models with a strong response, it does not emerge at all within the twenty-first century in the models with a weak response. This confirms that substantial uncertainty still characterizes future changes in the zonal wind in central Europe in winter (Woollings 2010).

This analysis enables identification of the signals and regions where observations might first be used to test the atmospheric circulation response to climate change. In particular, the signals with the earliest time of emergence in the models with a strong response are the weakening of the jet in the southeastern North Atlantic (including Iberia) in MJJASO, which is expected to emerge by 2020 (Fig. 4b), and the westward zonal wind change in North Africa in NDJFMA, which is expected to emerge by 2025 (Fig. 4d). Therefore, in these regions, it might soon be possible to test whether the model projections associated with the largest future responses are consistent with observations. This will enable to provide an upper bound on the most extreme projections.

Figure 4 also shows that the pooled variability simulated by the models (red horizontal line) is consistent with the variability observed in JRA-55 and ERAI in each of the four regions (vertical error bars). This suggests that there is no evidence of systematic biases in the variability of 30-yr

[1] To better sample the end-of-century response the average of the responses by 2080 and by 2100 is considered. The sensitivity of the results to this choice is small.

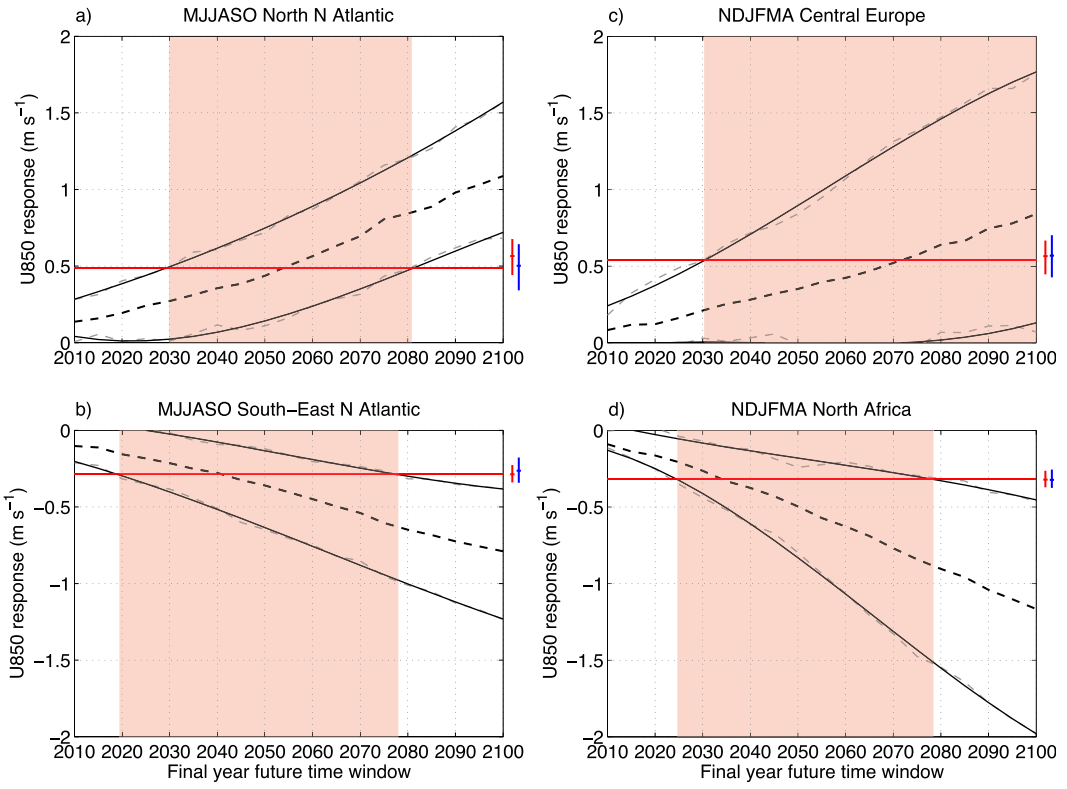

FIG. 4. Temporal evolution of the U850 response area–averaged in the (a) northern and (b) southeastern North Atlantic regions in MJJASO. The black dashed line gives the multimodel mean response. The gray dashed lines give the average of the subset of models with the 20% strongest and weakest end-of-century climate responses and the black solid lines are their third-order polynomial fit. The horizontal red line gives the noise level on the climate response due to internal variability in the climate models. The vertical error bars to the right indicate the 95% confidence interval on the noise level estimated from two atmospheric reanalyses: JRA-55 (red) and ERA-Interim (blue) (see appendix). The pink shading marks the uncertainty range on the time of emergence due to differences in the model responses. (c),(d) As in (a),(b), but for the area-averaged responses in central Europe and North Africa, respectively, in NDJFMA. The four regions are defined by the boxes indicated in Figs. 2c,d and 3c,d. The responses are evaluated for lead times 5 yr apart and interpolated in between.

means, which could otherwise affect the estimated time of emergence of climate change in the real world.

A summary of the model uncertainty on the time of emergence of the U850 response area averaged in the four study areas is reported in Table 2 for both the meteorological and the extended seasons. Extending the seasonal average is estimated to lead to an earlier time of emergence by up to 15 years in the models with a strong response and by up to 25 years in the models with a weak response. Central Europe in winter is the only region of the four where the response does not emerge within the twenty-first century in either DJF or NDJFMA according to the models with a weak climate response.

5. Signal-to-noise ratio and optimal seasonal averaging

In this section we propose a simple method to identify the optimal seasons for climate change detection in terms of the signal-to-noise ratio of the climate change response. To do this, a single-value measure of signal-to-noise ratio ($\overline{\beta/\sigma}$) in the North Atlantic and European area is now introduced. In particular, $\overline{\beta/\sigma}$ is defined as the root-mean-square of the signal-to-noise ratio in the North Atlantic and European region (20°–75°N, 80°W–40°E) and it is evaluated for the end-of-century climate change response.

Figure 5a shows $\overline{\beta/\sigma}$ evaluated for a set of different temporal averages. The largest signal-to-noise ratio is found for the extended summer season response (MJJASO), which is 25% higher than in JJA. The increase in $\overline{\beta/\sigma}$ from JJA to MJJASO is robust across the CMIP5 models as it is found in 31 of the 35 individual model responses (see Fig. 5b). Similarly, the signal-to-noise ratio of the extended winter response is about 30% higher than that found for DJF, and an increase in $\overline{\beta/\sigma}$ is found in 34 of the 35 individual model responses (see Fig. 5c). As the amplitude of the end-of-century U850 response is comparable in the meteorological and extended seasons (see Figs. 2a,b

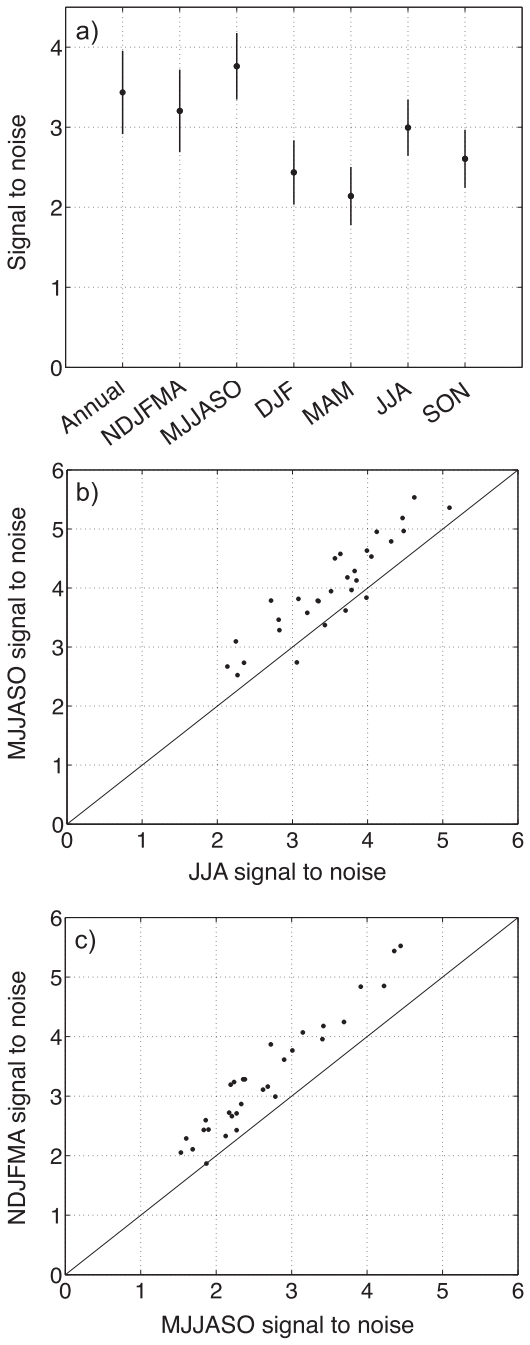

FIG. 5. (a) Area average signal-to-noise ratio ($\overline{\beta/\sigma}$) of the U850 multimodel mean end-of-century response separately evaluated for the annual mean, the two extended seasons, and the four meteorological seasons (MAM is March–May). The ratio $\overline{\beta/\sigma}$ is evaluated as the square root of the area average of the signal-to-noise ratio squared at the individual grid points in the North Atlantic and European area. The vertical bars indicate 95% confidence intervals on $\overline{\beta/\sigma}$ computed by bootstrap resampling with repetition over the CMIP5 models. (b) Scatterplot of $\overline{\beta/\sigma}$ evaluated for the extended summer response against the meteorological summer response in the individual CMIP5 models. (c) As in (b), but for the extended winter and meteorological winter seasons.

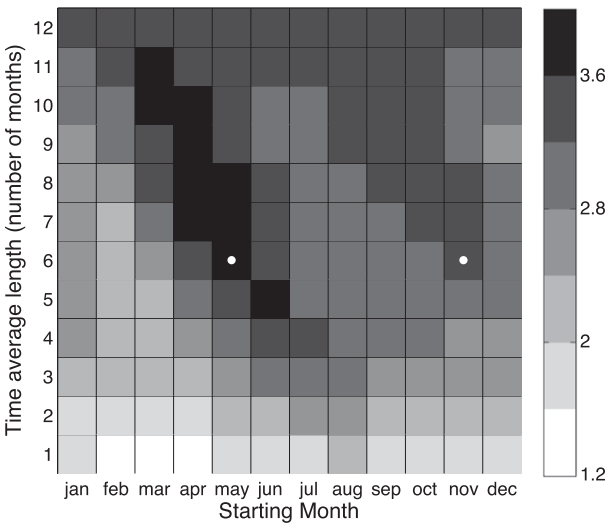

FIG. 6. Sensitivity of the signal-to-noise ratio ($\overline{\beta/\sigma}$) of the multimodel mean North Atlantic U850 response to the temporal average. The ratio $\overline{\beta/\sigma}$ is evaluated for the time mean response associated with all possible sequences of consecutive months within the annual cycle, and presented as a function of the starting month (x axis) and the temporal length (y axis) of the time average. The two white dots correspond to the two extended seasons that have been identified to capture best the future response of the North Atlantic jet.

and 3a,b), the increase in signal-to-noise ratio has to be related to a reduction in the noise.

Midlatitude atmospheric variability is dominated by weather regimes that typically vary on submonthly time scales. As a result, the fluctuations due to internal variability are weakly correlated across consecutive months and the noise is reduced by taking longer temporal averages. However, the signal-to-noise ratio will not necessarily increase as the signal can also be reduced by extending the temporal average. Consistently, Fig. 5a shows that the annual mean response is associated with a signal-to-noise ratio intermediate between that of the extended summer and the extended winter. The reason for this is that the extended summer and winter responses are characterized by different patterns, which are only marginally overlapping. Therefore, the annual mean response lacks important information on the seasonality of the climate change response and it does not improve the signal-to-noise ratio of the response either.

For a further exploration of the sensitivity of the signal-to-noise ratio to the temporal average employed, Fig. 6 shows $\overline{\beta/\sigma}$ evaluated for all possible time averages within the annual cycle. The values are presented as a function of the starting month of the time average (x axis) and of its time length (y axis). Figure 6 confirms that a longer time average does not necessarily lead to a higher signal-to-noise ratio. For example, the future response evaluated for a temporal average starting in June shows

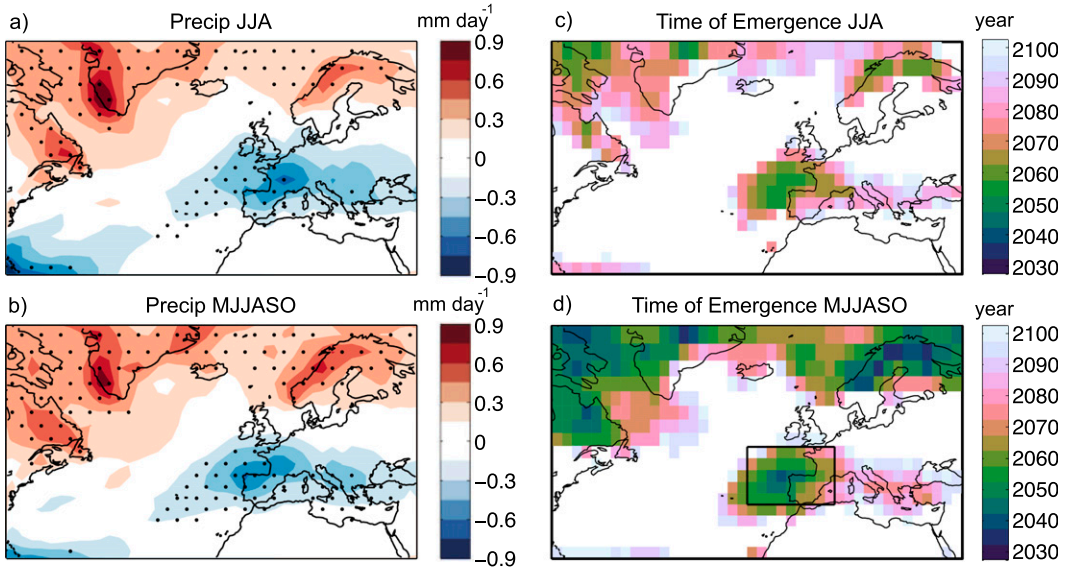

FIG. 7. As in Fig. 2, but for the multimodel mean precipitation response in JJA and MJJASO.

an increase in the signal-to-noise ratio for temporal averages extending up to 5 months (June–October) but a reduction afterward. Moreover, the extended spring (February–July) mean response is characterized by a low signal-to-noise ratio (<2.5) despite the 6-month time average. This largely results because responses of opposite signs are found in the different months of the time average, particularly in the Norwegian Sea and western Europe (see Fig. 1).

Among all the possible 6-month time averages, two distinct maxima in the signal-to-noise ratio are found at the starting months of May (MJJASO) and November (NDJFMA). This shows that the two extended seasons identified in this paper enable the identification of the seasonality of the climate change response and also maximize the signal-to-noise ratio of the climate response. More generally, these results suggest that recognizing the seasonality of the climate change response can be guided by the identification of the time periods that maximize the signal-to-noise ratio of the climate response.

Finally, we note that the ability to discern the two seasonal maxima in Fig. 6 can depend on how the area average signal-to-noise ratio $\overline{\beta/\sigma}$ is exactly computed. In particular, we find that the winter maximum becomes less prominent if $\overline{\beta/\sigma}$ is evaluated as the area average of the absolute values of signal-to-noise ratio (not shown), rather than as the root-mean-square. This happens because the wintertime response is spatially confined over Europe, so its signal-to-noise ratio is damped by an area average over the whole North Atlantic region. In contrast, the root-mean-square is equivalent to weighting the area average by the magnitude of the signal-to-noise ratio itself, therefore giving more weight to the regional responses.

6. Seasonality of the precipitation response

We now explore what seasonality is appropriate to detect the mean precipitation response to climate change. Because of the influence of the eddy-driven jet on precipitation, we first consider the same extended seasons identified for the U850 response and compare them with the meteorological seasons. However, precipitation can also directly respond to climate change via thermodynamic processes, with wet regions tending to become wetter and dry regions drier (Held and Soden 2006). The extent to which MJJASO and NDJFMA are optimal to detect precipitation changes will be verified using the diagnostic introduced in Fig. 6.

Figure 7a shows the multimean precipitation response in JJA. The response is characterized by increased precipitation at high latitudes, including Labrador, Greenland, and Scandinavia, and reduced precipitation in the southeastern North Atlantic and western Europe, particularly in Spain and France. A very similar spatial pattern is found in MJJASO (Fig. 7b), which suggests that little information is lost by considering the extended summer. Comparing Fig. 7c with Fig. 7d reveals that the time of emergence of the precipitation response is anticipated in MJJASO compared to JJA at nearly every grid point. This is particularly notable for the high-latitude precipitation increase, which emerges at least 20 years earlier in MJJASO (around 2050) compared with JJA (around 2070) at the individual grid points.

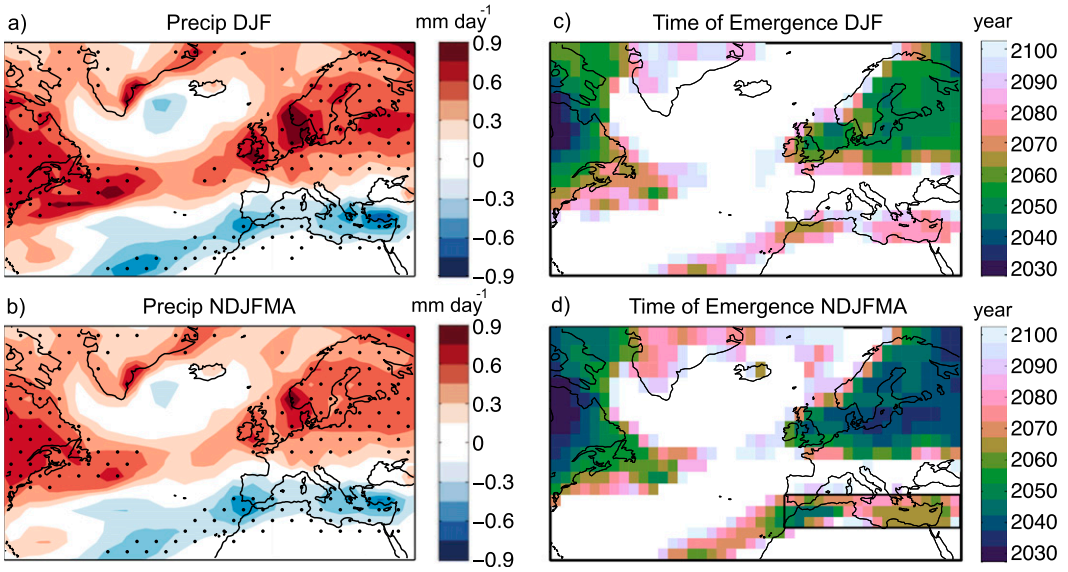

FIG. 8. As in Fig. 2, but for the multimodel mean precipitation response in DJF and NDJFMA.

The multimodel mean precipitation responses in DJF and NDJFMA are presented in Figs. 8a and 8b. In DJF, precipitation is projected to decrease in the Mediterranean area, and to increase in northeastern North America and most of northern Europe, including the British Isles. The precipitation response in the extended winter (NDJFMA) well resembles that found in DJF, although the amplitudes are locally slightly reduced. Despite the smaller signal, the time of emergence is still everywhere advanced by at least 15 years from DJF to NDJFMA (Figs. 8c and 8d). The high-latitude precipitation increase is expected to emerge before the precipitation reduction in the Mediterranean area.

While the meteorological and extended seasons show similar precipitation responses, some relevant differences are found between the extended summer (Fig. 7b) and the extended winter (Fig. 8b) responses. For example, in western Europe (i.e., southern England and France) precipitation is projected to increase in winter but decrease in summer, while the area affected by a precipitation reduction shifts from the Mediterranean area (NDJFMA) to western Europe (MJJASO). These results suggest that there is a seasonality in the European precipitation response to climate change, but are NDJFMA and MJJASO the best time averages to capture it?

To answer this question, Fig. 9a shows the sensitivity of the signal-to-noise ratio diagnostic ($\overline{\beta/\sigma}$) area averaged over Europe (30°–70°N, 10°W–40°E) to the choice of the temporal average. The highest signal-to-noise ratio is found for time averages starting in October–November and lasting 5–7 months. This includes the extended winter period defined above. Moreover, for a fixed 6-month time average, two separate maxima in $\overline{\beta/\sigma}$ are found for the starting months of May and November. The presence of these two distinct maxima in the signal-to-noise ratio of the response is more evident in Fig. 9b, where $\overline{\beta/\sigma}$ is evaluated for the central European and Mediterranean areas only (30°–53°N, 10°W–40°E). This confirms that MJJASO and NDJFMA are good choices to detect the European precipitation response, and particularly the southern European response.

The uncertainty on the time of emergence of the precipitation response in the southeastern North Atlantic (MJJASO) and in the Mediterranean area (NDJFMA) is now investigated in more detail. The projected precipitation reduction in these areas is of particular concern as it can lead to large socioeconomic impacts due to the susceptibility of Mediterranean countries to water stress. The precipitation responses are evaluated as area averages in the boxes indicated in Figs. 7d and 8d. The temporal evolution of these area-averaged responses is presented in Fig. 10. Note that the noise level from the models (red horizontal line) is found to be consistent with the two observational estimates.

The area-averaged precipitation reduction in MJJASO in the southeastern North Atlantic, including France and Spain, emerges by 2040 in the multimodel mean response (Fig. 10a). Furthermore, the strong and weak model response averages show an uncertainty range of about ±20 yr in the time of emergence (2025–60) due to model uncertainty. A similar uncertainty range is found for the time of emergence of the precipitation response in the Mediterranean area in NDJFMA (Fig. 10b). Therefore, CMIP5 models indicate that both regions will observe a

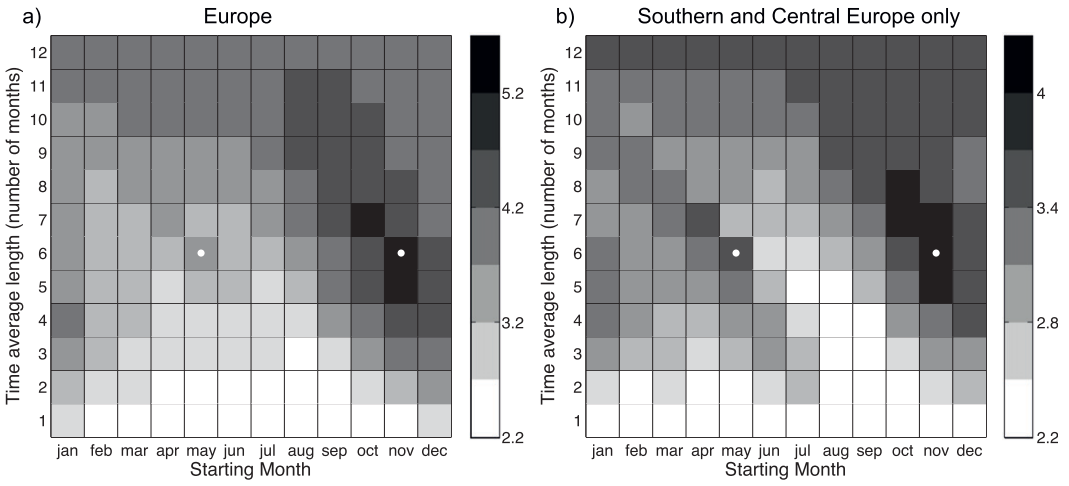

FIG. 9. As in Fig. 6, but for the signal-to-noise ratio $\overline{\beta/\sigma}$ of the multimodel mean precipitation response area averaged in (a) the European region (30°–70°N, 10°W–40°E) and (b) the central and southern European region only (30°–53°N, 10°W–40°E).

reduction in the time mean precipitation within the next 10–45 years relative to the 1960–90 climate.

In both regions, the end-of-century precipitation response differs by a factor of about 3 between the models with a strong and a weak response (see Figs. 10a,b). Reducing this uncertainty range would be important to plan adaptation policies. These results suggest that observations might soon be useful to test whether the projections from the models with the largest precipitation reductions, which should emerge by 2025, are realistic. This may enable us to provide an upper bound on the projected precipitation reduction. However, detecting these signals would require knowing the 1960–90 mean precipitation climatology, which might not be available in oceanic regions. We find that if the reference period is shifted to 1979–2009, when satellite-derived datasets become available, the emergence of the signals is postponed by about 10 years for the models with a strong response and about 5 years for the multimodel mean (not shown).

7. Conclusions

This study has explored the potential to use information on the seasonality of the North Atlantic jet and European precipitation response to climate change to improve their detection in the observations. The climate change response is evaluated in the CMIP5 models under the RCP8.5 scenario relative to the 1960–90 climatology.

The main findings of this study are the following:

- The climate change response in the zonal wind at 850 hPa is characterized by a well-defined seasonality, which is best described by two seasons. An extended summer season ranges from May to October (MJJASO), and in this period the North Atlantic jet tends to shift

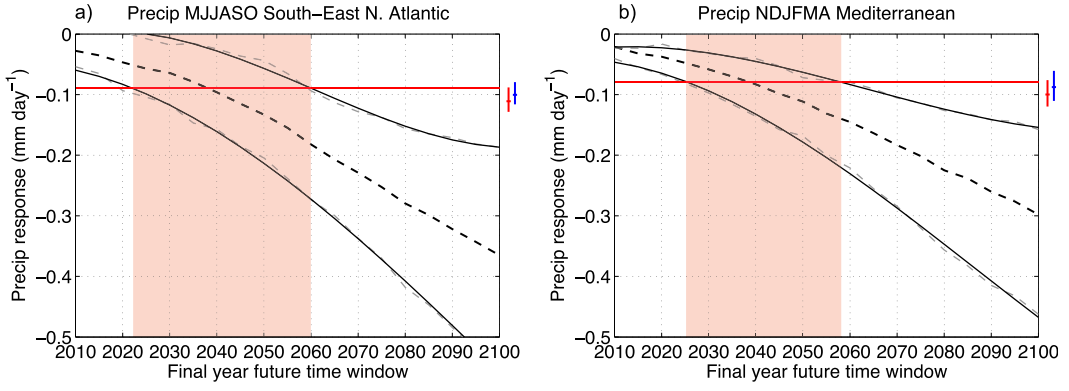

FIG. 10. (a) As in Fig. 4, but for the area-averaged precipitation in the southeastern North Atlantic in MJJASO (box in Fig. 7d) and (b) in the Mediterranean area in NDJFMA (box in Fig. 8d). The 95% confidence intervals on the noise level for the observed internal atmospheric variability are estimated from the GPCP (red) and CMAP (blue) datasets.

poleward. An extended winter season ranges from November to April (NDJFMA), and in this period the westerlies tend to intensity in central Europe, while a response of opposite sign is found in North Africa.

- The amplitude of the U850 climate change response (the signal) relative to the amplitude of the internal climate variability of 30-yr means (the noise) is 25%–30% higher in the extended seasons than in the corresponding meteorological seasons. This leads to a 5–15-yr earlier time of emergence of climate change depending on the region. These results suggest that considering the extended seasons will give a better ability to detect the projected climate change responses in the observations.
- According to the CMIP5 models, the U850 climate change response has not yet emerged from internal climate variability. This is consistent with the fact that, to our knowledge, no study has yet identified these signals in the observations.
- This study has identified two areas within the North Atlantic and European region where the climate change response in U850 can be expected to be detected first. These areas are the southeastern North Atlantic (including Iberia) in the extended summer and North Africa in the extended winter, which are both characterized by a westward wind change in the CMIP5 projections. In particular, these signals are projected to emerge by 2020 (southeastern North Atlantic) and by 2025 (North Africa) according to the average of the 20% of the models with the strongest future response. Therefore, observations might soon be useful to test these aspects of the atmospheric circulation response to climate change.
- MJJASO and NDJFMA are also optimal to capture the seasonality of the European precipitation response to climate change, leading to up to 10–20-yr earlier detection of the local precipitation responses. In particular, precipitation is projected to increase at the high latitudes, but to decline in both the southeastern North Atlantic and western Europe in MJJASO, and in the Mediterranean area in NDJFMA. The high-latitude precipitation increase is expected to emerge before the midlatitude reductions, and there are indications that it is already found in the observations (Zhang et al. 2007; Min et al. 2008; Balan Sarojini et al. 2012).
- The precipitation reduction in both the southeastern North Atlantic (MJJASO) and the Mediterranean area (NDJFMA) are projected to emerge between 2025 and 2060 according to the average of the models with the 20% strongest and weakest end-of-century precipitation responses. Therefore, it might soon be possible to test whether the models showing the largest future precipitation reductions are consistent with the observations.
- For both the North Atlantic jet and the European precipitation response, the signal-to-noise ratio in the annual mean is not higher than that found in the extended seasons and it further misses the information on the seasonality of the climate change response.

The 6-month extended seasons (NDJFMA and MJJASO) proposed here are not new in the climate change literature (e.g., Wallace et al. 2012; Iles et al. 2013; Seager et al. 2014). They represent a way to partition the year into a cold and a warm season, and to capture the seasonal cycle in both the atmospheric circulation (Peixoto and Oort 1992) and precipitation (Pascale et al. 2015) in the present-day climate. Here we have shown that this approach also represents the way to maximize the signal-to-noise ratio for the U850 and precipitation response to climate change in the North Atlantic and European region. The extent that this also applies to other regions and fields can be tested using the methodologies presented in this paper.

Deser et al. (2012), by analyzing a single climate model, suggested that regional precipitation and sea level pressure projections will be dominated by internal variability for at least 50 years. A direct comparison with our results is not possible due to the use of different climate models and greenhouse gas emission scenario, the use of a different reference period [2005–14 in Deser et al. (2012)] and of 10-yr rather than 30-yr means. Nonetheless, based on the CMIP5 models and using 1960–90 as reference period, we find that both the U850 and precipitation climate change responses could emerge regionally before 2050 in many areas. Crucially, once model uncertainty is taken into account, we further highlight that for some specific regions climate change might already emerge within the next decade according to the models with a strong climate response.

Some of the projected changes in U850 and precipitation are likely to be connected. In particular, the westward zonal wind change projected to occur in North Africa in NDJFMA is related to an increase in surface pressure and a reduction in the number of extratropical cyclones and precipitation in the Mediterranean area (Lionello et al. 2006; Giorgi and Lionello 2008; Seager et al. 2014; Zappa et al. 2015). Moreover, the poleward shift of the North Atlantic jet in MJJASO is expected to affect precipitation in southern England and northwestern France (Rowell and Jones 2006; Bladé et al. 2012). The potential to use the relationships between the atmospheric circulation and precipitation to improve the climate change detection of the precipitation responses will be addressed by future research.

Acknowledgments. We acknowledge the World Climate Research Programme's Working Group on Coupled Modelling, which is responsible for CMIP, and we thank the climate modeling groups (listed in Table 1 of this

paper) for producing and making available their model output. For CMIP the U.S. Department of Energy's Program for Climate Model Diagnosis and Intercomparison provides coordinating support and led development of software infrastructure in partnership with the Global Organisation for Earth System Science Portals. We also thank the European Centre for Medium-Range Weather Forecasts for the ERA-Interim data and the Japan Meteorological Agency for JRA-55 data. The GPCP and CMAP datasets were provided by the NOAA/OAR/ESRL PSD, Boulder, Colorado, from their website at http://www.esrl.noaa.gov/psd/. We are also grateful to two anonymous reviewers and Gabi Hegerl for their constructive reviews. This study is supported by the "Understanding the atmospheric circulation response to climate change" (ACRCC, ERC Advanced Grant) project.

APPENDIX

Estimating the Noise due to Internal Variability

a. In the multimodel ensemble

Following Sansom et al. (2013), a single estimate of internal variability on the 30-yr mean climate is estimated for the whole multimodel ensemble under the assumption that the different models have the same variability. In particular, we define $y_{mr}(t)$ to be the 30-yr mean climate ending on year t for model m and ensemble member r. Also, we define $y_{mr}(t_H)$ as the reference 30-yr average in the historical period (1960–90). The variance σ^2 on the 30-yr mean climate due to internal climate variability can be estimated as

$$\sigma^2 = \frac{1}{N-M}\sum_{m=1}^{M}\left\{\sum_{r=1}^{R_{Hm}}[y_{mr}(t_H)-y_m(t_H)]^2\right\}, \qquad \text{(A1)}$$

where N is the total number of ensemble members in the historical simulations, M is the total number of models, R_{Hm} is the number of ensemble members in model m in the historical period, and y_m is the ensemble average across the members of model m.

Concerning the assumption of equal model variability, only limited evidence of intermodel differences in σ^2 has been found by applying the statistical techniques indicated in Sansom et al. (2013). Moreover, the time of emergence of climate change in the real world, which is the quantity of interest, will be determined by the amplitude of the observed, rather than modeled, climate variability. Therefore, the key question is whether the pooled model variability (σ^2) is consistent with the observed variability (see below). If that is the case, the presence of differences in the variability simulated by each model is a question of secondary relevance and the pooled model variability (σ^2) can be taken as a best estimate.

The impact of climate change on variability can be tested by reevaluating σ^2 using the 30-yr mean climate at the end of the twenty-first century (2070–2100) under the RCP8.5 scenario. For the specific areas and variables examined in this paper (Figs. 4 and 10), the change in σ is sufficiently small (no more than 10%) to impact the time of emergence for less than 5 years. Therefore, we find it acceptable to simply use the present-day climate variability to estimate the time of emergence of climate change.

b. In the observations

Because of the shortness of the observational records, estimates of the variability of 30-yr mean climate from the observations have to be inferred from the interannual variability. For the regional analyses presented in this paper (Figs. 4 and 10), we do not find strong evidence of significant autocorrelation in the interannual variability at any lag. Therefore, the variance of a 30-yr mean time average in the observations (σ^2_{obs}) is simply estimated as

$$\sigma^2_{\text{obs}} = \frac{s^2}{N_y}, \qquad \text{(A2)}$$

where N_y is the number of years in the time series and s^2 is the sample interannual variance. The 95% confidence interval on σ^2_{obs} is estimated by applying Eq. (A2) to 10 000 bootstrap samples with repetition of the observed time series, and by taking the 2.5th and 97.5th percentiles of the bootstrap distribution.

REFERENCES

Adler, R. F., and Coauthors, 2003: The version-2 Global Precipitation Climatology Project (GPCP) monthly precipitation analysis (1979–present). *J. Hydrometeor.,* **4,** 1147–1167, doi:10.1175/1525-7541(2003)004<1147:TVGPCP>2.0.CO;2.

Balan Sarojini, B., P. A. Stott, E. Black, and D. Polson, 2012: Fingerprints of changes in annual and seasonal precipitation from CMIP5 models over land and ocean. *Geophys. Res. Lett.,* **39,** L21706, doi:10.1029/2012GL053373.

Barkhordarian, A., H. von Storch, and J. Bhend, 2013: The expectation of future precipitation change over the Mediterranean region is different from what we observe. *Climate Dyn.,* **40,** 225–244, doi:10.1007/s00382-012-1497-7.

Barnes, E. A., and L. Polvani, 2013: Response of the midlatitude jets, and of their variability, to increased greenhouse gases in the CMIP5 models. *J. Climate,* **26,** 7117–7135, doi:10.1175/JCLI-D-12-00536.1.

Barnett, T., and Coauthors, 2005: Detecting and attributing external influences on the climate system: A review of recent advances. *J. Climate,* **18,** 1291–1314, doi:10.1175/JCLI3329.1.

Bindoff, N. L., and Coauthors, 2013: Detection and attribution of climate change: From global to regional. *Climate Change 2013:*

The Physical Science Basis, T. Stocker et al., Eds., Cambridge University Press, 867–952.

Bladé, I., D. Fortuny, G. J. van Oldenborgh, and B. Liebmann, 2012: The summer North Atlantic Oscillation in CMIP3 models and related uncertainties in projected summer drying in Europe. *J. Geophys. Res.,* **117,** D16104, doi:10.1029/2012JD017816.

Chang, E. K., Y. Guo, and X. Xia, 2012: CMIP5 multimodel ensemble projection of storm track change under global warming. *J. Geophys. Res.,* **117,** D23118, doi:10.1029/2012JD018578.

Christensen, J. H., and Coauthors, 2007: Regional climate projections. *Climate Change 2007: The Physical Science Basis,* S. Solomon et al., Eds., Cambridge University Press, 847–940.

Dee, D. P., and Coauthors, 2011: The ERA-Interim reanalysis: Configuration and performance of the data assimilation system. *Quart. J. Roy. Meteor. Soc.,* **137,** 553–597, doi:10.1002/qj.828.

Deser, C., A. Phillips, V. Bourdette, and H. Teng, 2012: Uncertainty in climate change projections: The role of internal variability. *Climate Dyn.,* **38,** 527–546, doi:10.1007/s00382-010-0977-x.

——, A. S. Phillips, M. A. Alexander, and B. V. Smoliak, 2014: Projecting North American climate over the next 50 years: Uncertainty due to internal variability. *J. Climate,* **27,** 2271–2296, doi:10.1175/JCLI-D-13-00451.1.

Gillett, N. P., and P. A. Stott, 2009: Attribution of anthropogenic influence on seasonal sea level pressure. *Geophys. Res. Lett.,* **36,** L23709, doi:10.1029/2009GL041269.

——, F. W. Zwiers, A. J. Weaver, and P. A. Stott, 2003: Detection of human influence on sea-level pressure. *Nature,* **422,** 292–294, doi:10.1038/nature01487.

——, R. J. Allan, and T. J. Ansell, 2005: Detection of external influence on sea level pressure with a multi-model ensemble. *Geophys. Res. Lett.,* **32,** L19714, doi:10.1029/2005GL023640.

Giorgi, F., and P. Lionello, 2008: Climate change projections for the Mediterranean region. *Global Planet. Change,* **63,** 90–104, doi:10.1016/j.gloplacha.2007.09.005.

——, and X. Bi, 2009: Time of emergence (TOE) of GHG-forced precipitation change hot-spots. *Geophys. Res. Lett.,* **36,** L06709, doi:10.1029/2009GL037593.

Hawkins, E., and R. Sutton, 2009: The potential to narrow uncertainty in regional climate predictions. *Bull. Amer. Meteor. Soc.,* **90,** 1095–1107, doi:10.1175/2009BAMS2607.1.

——, and ——, 2012: Time of emergence of climate signals. *Geophys. Res. Lett.,* **39,** L01702, doi:10.1029/2011GL050087.

Hegerl, G. C., K. Hasselmann, U. Cubasch, J. Mitchell, E. Roeckner, R. Voss, and J. Waszkewitz, 1997: Multi-fingerprint detection and attribution analysis of greenhouse gas, greenhouse gas-plus-aerosol and solar forced climate change. *Climate Dyn.,* **13,** 613–634, doi:10.1007/s003820050186.

Held, I., and B. Soden, 2006: Robust responses of the hydrological cycle to global warming. *J. Climate,* **19,** 5686–5699, doi:10.1175/JCLI3990.1.

Iles, C. E., G. C. Hegerl, A. P. Schurer, and X. Zhang, 2013: The effect of volcanic eruptions on global precipitation. *J. Geophys. Res. Atmos.,* **118,** 8770–8786, doi:10.1002/jgrd.50678.

Jones, P. W., 1999: First- and second-order conservative remapping schemes for grids in spherical coordinates. *Mon. Wea. Rev.,* **127,** 2204–2210, doi:10.1175/1520-0493(1999)127<2204:FASOCR>2.0.CO;2.

Kobayashi, S., and Coauthors, 2015: The JRA-55 Reanalysis: General specifications and basic characteristics. *J. Meteor. Soc. Japan,* **93,** 5–48, doi:10.2151/jmsj.2015-001.

Lionello, P., and Coauthors, 2006: The Mediterranean climate: An overview of the main characteristics and issues. *Dev. Earth Environ. Sci.,* **4,** 1–26, doi:10.1016/S1571-9197(06)80003-0.

Mahlstein, I., R. Knutti, S. Solomon, and R. Portmann, 2011: Early onset of significant local warming in low latitude countries. *Environ. Res. Lett.,* **6,** 034009, doi:10.1088/1748-9326/6/3/034009.

Marvel, K., and C. Bonfils, 2013: Identifying external influences on global precipitation. *Proc. Natl. Acad. Sci. USA,* **110,** 19 301–19 306, doi:10.1073/pnas.1314382110.

Min, S.-K., X. Zhang, and F. Zwiers, 2008: Human-induced Arctic moistening. *Science,* **320,** 518–520, doi:10.1126/science.1153468.

Noake, K., D. Polson, G. Hegerl, and X. Zhang, 2012: Changes in seasonal land precipitation during the latter twentieth-century. *Geophys. Res. Lett.,* **39,** L03706, doi:10.1029/2011GL050405.

Osborn, T. J., 2004: Simulating the winter North Atlantic Oscillation: The roles of internal variability and greenhouse gas forcing. *Climate Dyn.,* **22,** 605–623, doi:10.1007/s00382-004-0405-1.

Palmer, T. N., 1999: A nonlinear dynamical perspective on climate prediction. *J. Climate,* **12,** 575–591, doi:10.1175/1520-0442(1999)012<0575:ANDPOC>2.0.CO;2.

Pascale, S., V. Lucarini, X. Feng, A. Porporato, and S. ul Hasson, 2015: Analysis of rainfall seasonality from observations and climate models. *Climate Dyn.,* **44,** 3281–3301, doi:10.1007/s00382-014-2278-2.

Peixoto, J., and A. Oort, 1992: *Physics of Climate.* American Institute of Physics, 520 pp.

Pinto, J. G., E. Fröhlich, G. Leckebusch, and U. Ulbrich, 2007: Changing European storm loss potentials under modified climate conditions according to ensemble simulations of the ECHAM5/MPI-OM1 GCM. *Nat. Hazards Earth Syst. Sci.,* **7,** 165–175, doi:10.5194/nhess-7-165-2007.

——, M. K. Karremann, K. Born, P. M. Della-Marta, and M. Klawa, 2012: Loss potentials associated with European windstorms under future climate conditions. *Climate Res.,* **54,** 1–20, doi:10.3354/cr01111.

Rowell, D. P., and R. G. Jones, 2006: Causes and uncertainty of future summer drying over Europe. *Climate Dyn.,* **27,** 281–299, doi:10.1007/s00382-006-0125-9.

Sansom, P. G., D. B. Stephenson, C. A. Ferro, G. Zappa, and L. Shaffrey, 2013: Simple uncertainty frameworks for selecting weighting schemes and interpreting multimodel ensemble climate change experiments. *J. Climate,* **26,** 4017–4037, doi:10.1175/JCLI-D-12-00462.1.

Seager, R., H. Liu, N. Henderson, I. Simpson, C. Kelley, T. Shaw, Y. Kushnir, and M. Ting, 2014: Causes of increasing aridification of the Mediterranean region in response to rising greenhouse gases. *J. Climate,* **27,** 4655–4676, doi:10.1175/JCLI-D-13-00446.1.

Semenov, V. A., M. Latif, J. H. Jungclaus, and W. Park, 2008: Is the observed NAO variability during the instrumental record unusual? *Geophys. Res. Lett.,* **35,** L11701, doi:10.1029/2008GL033273.

Shepherd, T. G., 2014: Atmospheric circulation as a source of uncertainty in climate change projections. *Nat. Geosci.,* **7,** 703–708, doi:10.1038/ngeo2253.

Shindell, D. T., R. L. Miller, G. A. Schmidt, and L. Pandolfo, 1999: Simulation of recent northern winter climate trends by greenhouse-gas forcing. *Nature,* **399,** 452–455, doi:10.1038/20905.

Simpson, I. R., T. A. Shaw, and R. Seager, 2014: A diagnosis of the seasonally and longitudinally varying midlatitude circulation response to global warming. *J. Atmos. Sci.,* **71,** 2489–2515, doi:10.1175/JAS-D-13-0325.1.

Stott, P. A., 2003: Attribution of regional-scale temperature changes to anthropogenic and natural causes. *Geophys. Res. Lett.,* **30,** 1724, doi:10.1029/2003GL017324.

Taylor, K., R. Stouffer, and G. Meehl, 2012: An overview of CMIP5 and the experiment design. *Bull. Amer. Meteor. Soc.,* **93,** 485–498, doi:10.1175/BAMS-D-11-00094.1.

Wallace, J. M., Q. Fu, B. V. Smoliak, P. Lin, and C. M. Johanson, 2012: Simulated versus observed patterns of warming over the extratropical Northern Hemisphere continents during the cold season. *Proc. Natl. Acad. Sci. USA,* **109,** 14 337–14 342, doi:10.1073/pnas.1204875109.

Woollings, T., 2010: Dynamical influences on European climate: An uncertain future. *Philos. Trans. Roy. Soc.,* **368A,** 3733–3756, doi:10.1098/rsta.2010.0040.

——, A. Hannachi, and B. Hoskins, 2010: Variability of the North Atlantic eddy-driven jet stream. *Quart. J. Roy. Meteor. Soc.,* **136,** 856–868, doi:10.1002/qj.625.

Xie, P., and P. A. Arkin, 1997: Global precipitation: A 17-year monthly analysis based on gauge observations, satellite estimates, and numerical model outputs. *Bull. Amer. Meteor. Soc.,* **78,** 2539–2558, doi:10.1175/1520-0477(1997)078<2539:GPAYMA>2.0.CO;2.

Zappa, G., L. C. Shaffrey, K. I. Hodges, P. G. Sansom, and D. B. Stephenson, 2013: A multimodel assessment of future projections of North Atlantic and European extratropical cyclones in the CMIP5 climate models. *J. Climate,* **26,** 5846–5862, doi:10.1175/JCLI-D-12-00573.1.

——, M. K. Hawcroft, L. Shaffrey, E. Black, and D. J. Brayshaw, 2015: Extratropical cyclones and the projected decline of winter Mediterranean precipitation in the CMIP5 models. *Climate Dyn.,* doi:10.1007/s00382-014-2426-8, in press.

Zhang, X., F. W. Zwiers, G. C. Hegerl, F. H. Lambert, N. P. Gillett, S. Solomon, P. A. Stott, and T. Nozawa, 2007: Detection of human influence on twentieth-century precipitation trends. *Nature,* **448,** 461–465, doi:10.1038/nature06025.